

Simulations of single grafted polyelectrolyte chains: ssDNA and dsDNA

Paul S. Crozier^{a)} and Mark J. Stevens

Sandia National Laboratories, P.O. Box 5800, MS 0316, Albuquerque, New Mexico 87185-0316

(Received 11 September 2002; accepted 2 December 2002)

The structure of a single, grafted polyelectrolyte, DNA, is investigated by molecular dynamics simulations. The polyelectrolyte is treated as a bead–spring model with explicit charges using parametrizations of both flexible (ssDNA) and stiff (dsDNA) polyelectrolytes. In this single chain limit with no added salt, the flexible ssDNA is always highly extended. Counterion condensation on both molecules is found to be chain length dependent. The counterion distribution is not localized to the chain volume as in related polyelectrolyte brush states. Even at large chain lengths, where the majority of counterions are condensed, a significant fraction of counterions reside far from the chain. The distributions of positions of the nongrafted end monomer for ssDNA and dsDNA differ significantly, indicating a possibility for distinguishing the two states in DNA array technologies. © 2003 American Institute of Physics. [DOI: 10.1063/1.1540098]

I. INTRODUCTION

The grafting of DNA strands to surfaces in microarrays has recently revolutionized DNA sequencing. The development of microarrays has occurred without much attention paid to the statistical conformations of the grafted DNA.^{1,2} An understanding of DNA conformations will aid further developments of DNA array-based sensors. In addition, grafted DNA is a subset of grafted polyelectrolytes, which have important applications. For instance, polyelectrolyte brushes are a key ingredient in the stabilization of colloids in aqueous solution.³ Also, many proteins are now realized to have segments, often end segments, that are unstructured, i.e., do not fold.⁴ These segments typically have amino acid sequences containing repeating motifs that generally involve charged amino acids. These unstructured tails can behave like grafted polyampholytes or polyelectrolytes depending on the charge distribution.^{5,6}

Here, we extend our coarse-grained model of polyelectrolytes in solution^{7,8} to treat a single polyelectrolyte chain grafted to a solid surface. Molecular dynamics (MD) simulations are performed using this model to calculate the chain structure and ionic distributions. These simulations lay the ground work for future multiple, grafted chain systems. We emphasize that the model is applicable to a variety of grafted polyelectrolytes. We parametrize our model to treat single-stranded DNA (ssDNA) and double-stranded DNA (dsDNA) as specific examples of strong polyelectrolytes.

There has been much theoretical work on polyelectrolyte brushes,^{9–13} yet it mostly focused on weak polyelectrolytes, not strong polyelectrolytes such as DNA. Theoretical approximations (i.e., Debye–Hückel, Poisson–Boltzmann) typically used are suspect for strong polyelectrolytes, of which DNA is an archetype. These approximations assume the electrostatic interactions are weak in comparison with the thermal energy, kT , which is false by definition of a strong polyelectrolyte. Molecular simulations can avoid issues of

these approximations by completely treating all the ionic interactions. Some such simulation work^{14–16} has been done on polyelectrolyte brushes, while very little simulation work has been done on isolated, constrained polyelectrolyte chains such as grafted DNA.⁶

Even though there is considerable interest in polyelectrolyte brushes and grafted DNA, only a small amount of experimental data exists to test the theoretical efforts. Well controlled experimental systems have been difficult to achieve, at least until recently.^{17–19} Polyelectrolyte brushes composed of poly(styrene sulfonate) have been made by initially grafting a neutral polystyrene brush and subsequently sulfonating it to obtain the polyelectrolyte.¹⁹ DNA has been grafted onto gold surfaces using thiol chemistry.² Alkanethiol molecules are end-attached to DNA which will then self-assemble via thiol chemistry onto a gold substrate. These grafted DNA systems offer the potential for the development of a well-controlled model of a grafted polyelectrolyte system.

In the following section, we detail the grafted polyelectrolyte model and the coarse-grained MD simulation procedure. Then we give results of the grafted dsDNA and ssDNA simulations with and without added salt, elucidating counterion condensation behavior and chain structure as a function of chain length and salt concentration. We conclude with a general discussion and possible directions for future work on simulation of grafted DNA.

II. SIMULATION DETAILS

Polyelectrolyte chains were modeled by a bead–spring polymer model that has been described elsewhere in the literature.^{6–8} The bead–bead interaction is given by the Lennard-Jones (LJ) potential,

$$U_{LJ}(r) = \begin{cases} 4\epsilon \left[\left(\frac{d}{r} \right)^{12} - \left(\frac{d}{r} \right)^6 + \frac{1}{4} \right], & r \leq r_c, \\ 0, & r > r_c, \end{cases} \quad (1)$$

where d is the bead diameter in multiples of σ , the LJ unit of length, and ϵ is the LJ unit of energy. Since water is a good

^{a)}Electronic mail: pscrozi@sandia.gov

TABLE I. System parameters.

System	a	σ	d	ξ
ssDNA	3.4 Å	3.09 Å	1.29 σ	4.2
dsDNA	1.7 Å	1.54 Å	2.60 σ	2.1

solvent for polyelectrolytes, the LJ potential is cutoff at $r_c = 2^{1/6}d$, yielding a purely repulsive interaction. This same interaction is used for all pair interactions (counterion–monomer, etc.).

The bond potential is the sum of the repulsive LJ potential and the attractive FENE (finite extensible, nonlinear elastic) potential.

$$U_{\text{bond}}(r) = -1/2kR_0^2 \ln(1 - r^2/R_0^2), \quad (2)$$

with spring constant $k = 7\epsilon/\sigma^2$, and maximum extent, $R_0 = 2\sigma$. Given this bond interaction, the average bond length will be $a = 1.1\sigma$.

Molecules of ssDNA and dsDNA are also differentiated by the angle flexibility term,

$$U_{\text{angle}} = k_\theta(\theta - \theta_0)^2, \quad (3)$$

where k_θ is the angle stiffness term and θ is the bond angle in degrees. Flexible ssDNA were modeled with $k_\theta = 0$ for the angle term, whereas dsDNA chains were modeled with $k_\theta = 300\epsilon/\text{rad}^2$ and $\theta_0 = 180^\circ$ to yield the correct persistence length.

Polymer beads, coions and counterions are all monovalent. Each bead represents one DNA monomer in the N -bead polymer chain (phosphate, base, and sugar) with its corresponding charge of $-e$. Charged particles interact according to the Coulomb potential

$$u_{ij}(r) = z_i z_j k_B T \lambda / r, \quad (4)$$

where z_i is the charge valence on particle i and the Bjerrum length in water is $\lambda = 7.1$ Å. The bond length, a , that characterizes the distance between beads of the chain, has been mapped to the DNA base charge separations of 3.4 Å for ssDNA and 1.7 Å for dsDNA. The conversion between LJ units and Å is obtained from the value of bond length, $a = 1.1\sigma$ and is given in Table I. In all the LJ pair interactions, d is taken to be 4 Å, which is a typical value used in primitive model electrolytes.

The solvent is treated at the primitive model level, setting the Bjerrum length to water's characteristic value of 7.1 Å. This is appropriate for most aspects of polyelectrolyte structure.⁷ The focus of this work is on the electrostatic interactions in competition with entropy. We neglect the intrinsically strong H bonds between complementary base pairs in ssDNA, because we are focusing on the polyelectrolyte nature of the structure. Furthermore, for chain lengths of interest the likelihood of self-hybridization is small. As will be seen, the electrostatic repulsion between the charged monomers results in a highly extended structure without the self-contact that H-bonding would require.

The simulated systems are periodic in the x and the y directions. But the accessible z -direction domain is nonperiodic with a wall at the grafting surface ($z=0$) and an addi-

tional wall at $z=L_z$, where L_z is the simulated slab thickness. Walls were modeled using the same repulsive LJ interactions as given in Eq. (1) above,

$$U_{\text{wall}}(z) = U_{\text{LJ}}(z). \quad (5)$$

Long-range electrostatics were treated by the P³M mesh-Ewald method,²⁰ with empty space left between periodically repeating slabs in the z direction, perpendicular to the grafting surface. A slab-geometry correction term was also included in order to damp out interslab interactions and model an isolated slab of fluid. This method has been shown to accurately treat long-range slab-geometry electrostatic interactions.^{21,22}

The total energy for the model system is

$$U_{\text{tot}} = U_{\text{LJ}} + U_{\text{bond}} + U_{\text{angle}} + U_{\text{Coulomb}} + U_{\text{wall}}. \quad (6)$$

Simulations without salt were performed at a dilute monomer density of 10^{-6} ions/ σ^3 in the particle-accessible portion of the simulation box. Beyond the cubic particle-accessible portion of the simulation box with dimensions $L_x = L_y = L_z$, an additional empty volume of $L_x \times L_y \times 2L_z$ was included between periodically repeating images of the slabs as per the slab-geometry simulation protocol cited above, yielding a total simulation box volume of $L_x \times L_y \times 3L_z$. Three salt concentrations were explored for the ssDNA case corresponding to 5 mM, 10 mM, and 20 mM. For each simulation 10^7 time steps of 0.01τ each were performed, where τ is the LJ time. In all cases, a Langevin thermostat with damping constant $\gamma = 1$ was used to maintain a temperature of $T = 1.0\epsilon$.

Chains were grafted to the surface by tethering the first bead of the chain to a “zeroth” bead that was uncharged and fixed in space at a distance of r_c from the left wall ($x=0, y=0, z=r_c$). Simulation of single isolated chains approximates the low polyelectrolyte concentration limit. Polymer chains of length $N = 16, 20, 32, 64, 128, \text{ and } 256$ were simulated.

Initial configurations for each system were created by randomly placing particles within the simulation cell constrained by the requirements that (1) chains start at the grafting point, (2) neighboring beads on polymer chains were at the equilibrium bond distance, (3) chains were stretched to near full extension, (4) all particles started between the walls, at a distance of at least r_c from both walls, (5) counterions were started within 5σ of the polymer chain.

III. RESULTS

The end-to-end distance, R , is a key measure of polymer structure. The calculation of R provides a check of the simulations, as well as a means to compare the two different systems. For strong polyelectrolytes such as DNA, we expect the scaling relation $R \sim N^\nu$ to have $\nu \approx 1$. In addition, since our values of N are below the corresponding persistence length for dsDNA, ν should be 1 in this case. Figure 1 shows that this is indeed the case. For the flexible single-stranded case, the value of ν is the same, but the magnitude of R is lower due to the difference in the chain flexibility. For $N = 20$ we also include a point with added salt for ssDNA. As

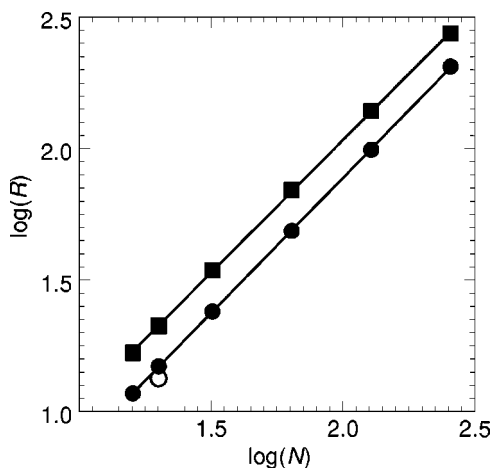


FIG. 1. End-to-end distance, R , as a function of chain length, N , for both dsDNA (boxes) and ssDNA (circles). All points are for simulations of a single grafted DNA molecule with counterions sufficient to neutralize the net charge of the chain, except the empty circle point which corresponds to ssDNA with compensating counterions and 10 mM salt. In both cases, the slope, which equals ν , is 1.

expected R decreases with added salt. Also, as noted in the beginning, the ssDNA structure is very extended so that intramolecular H bonds are not likely.

The properties of grafted polyelectrolytes are intimately related to the ion distributions. Figure 2 compares monomer, counterion, and salt density distributions in the direction perpendicular to the grafting surface (the z direction) for the $N=20$ case. The distributions are normalized such that $\int_0^{L_z} g(z) dz / (L_z N) = 1$, where $g(z)$ is the normalized density. Parts (a) and (b) compare results for ssDNA and dsDNA, respectively. The dsDNA monomer distribution has multiple well-resolved oscillations near the grafting surface wall. This is because dsDNA is stiff and the positions of these monomers close to the grafting site do not fluctuate much. For monomers further down the chain, pivoting about the grafting site yields significant lateral fluctuations. For this reason, $g(z)$ decreases monotonically for $z \geq 10\sigma$, as the lateral fluctuations increase with z . Since ssDNA is flexible, the oscillations do not appear at low z . Because R is larger for dsDNA and g is normalized, the ssDNA curve has a larger peak at low z . Otherwise, beyond the initial peak the ssDNA distribution similarly decreases with increasing z until reaching values beyond the contour length where $g=0$.

One of the basic questions for grafted polyelectrolytes is how the counterions are arranged. Specifically, how are the counterions split between being within the chain volume and outside of the chain volume? Here, we take the chain volume to be defined as the volume with $z \leq a(N-1)$. The counterion distributions in Fig. 2 show the main peak within the chain volume and a tail at larger z . For both ssDNA and dsDNA the peak height in the counterion distribution is much smaller than in the monomer distribution implying that the number of counterions within the chain volume is a small fraction of the total number. Table II shows the time-averaged value of the fraction of counterions within the chain volume. Both cases have values below 0.5 for this N . Thus, most of the counterions are located at values of z be-

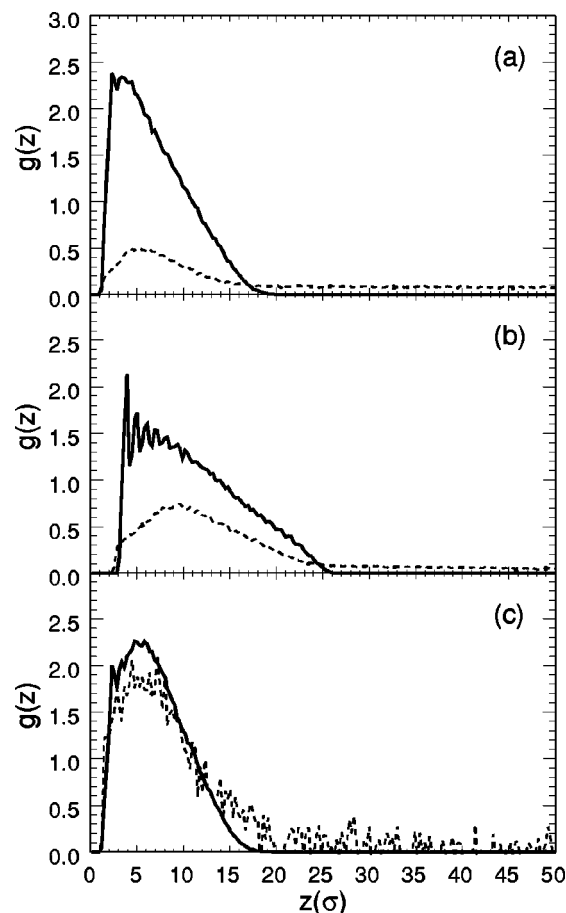


FIG. 2. Monomer (thick line) and counterion (dotted line) distributions as a function of distance from the grafting surface for $N=20$ chains of (a) ssDNA without salt, (b) dsDNA without salt, and (c) ssDNA in 5 mM salt. Net counterion (counterion-coion) density is plotted for (c). Densities have been normalized and plotted as the average number density of each species per unit length.

yond the chain length for this N . As N increases, the fraction of counterions within the chain volume increases as shown in Table II. This increase is related to the number of condensed counterions, as we discuss shortly.

The distributions for $N=64$ are shown in Fig. 3. The larger N has a qualitative difference in the distributions. The maximum occurs over a plateau region instead of at a peak. This is stronger in dsDNA than in ssDNA. For dsDNA, $g(z)$ has the same oscillations at small z as seen for the $N=20$

TABLE II. Fraction of counterions within $a(N-1)$ of the grafting surface. Statistics for salt runs are for the net number of counterions, i.e., (counterions-coions)/ N .

N	Salt conc. (mM)	ssDNA	dsDNA
16	0	0.22	0.38
20	0	0.25	0.45
20	5	0.84	
20	10	0.87	
20	20	0.97	
32	0	0.37	0.58
64	0	0.54	0.68
128	0	0.65	0.80
256	0	0.71	0.81

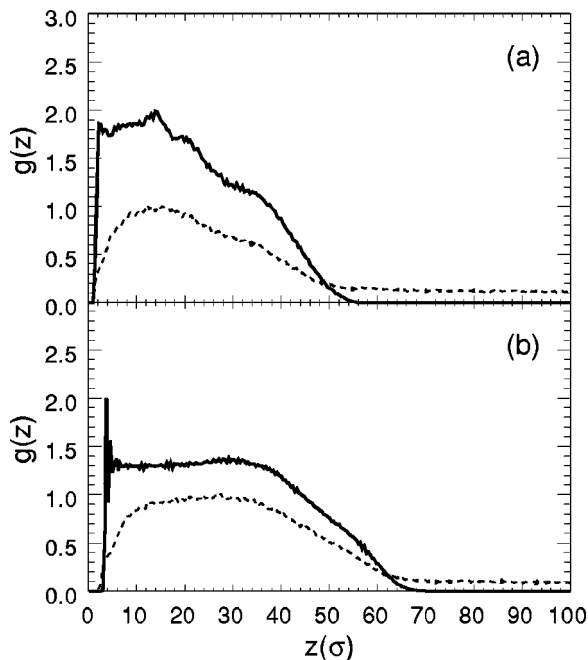


FIG. 3. Monomer (thick line) and counterion (dotted line) distributions as a function of distance from the grafting surface for $N=64$ chains of (a) ssDNA and (b) dsDNA.

case, then a long plateau to about $z=35\sigma$ and a drop thereafter to zero at about $z=65\sigma$. The long plateau occurs because dsDNA is stiff and, on average, there is approximately one monomer per unit length in the z direction. Different configurations for dsDNA are just different tilts about the grafting point. For a configuration at a given tilt angle θ with respect to the z axis, there are no monomers for $z > a(N-1)\cos\theta$. The drop-off at $z \approx 35\sigma$ implies that the largest tilt is about 60° in this case.

Noticeable differences occur in the distribution for ssDNA due to its flexibility. The value of $g(z)$ for low z is larger in ssDNA than in dsDNA, because the ssDNA can bend so that more than one monomer is at the same z . These curved configurations lead to the drop off occurring at a lower value, $z \approx 20\sigma$.

Before discussing the counterion distributions in Fig. 3, we note that for large N the fluctuations in the monomer $g(z)$ become successively more significant. Comparing different quartiles of a 10^7 step run showed significant fluctuations about the mean. Because of the low density the counterion dynamics becomes slower as L_z increases with N . This puts a limit on accurate calculation of $g(z)$ to $N \leq 128$. Other quantities (e.g., Table II) can be calculated accurately to $N=256$.

The counterion distributions in Fig. 3 tend to mirror the monomer distributions. Both dsDNA and ssDNA at $N=64$ have peaks at $g=1$ which is larger than the corresponding value at $N=20$. This larger value indicates the larger degree of counterion condensation (cf. Table II). As the table shows by $N=64$ the number of counterions within the chain volume is larger than outside the volume. Yet, there is still a long tail in the counterion distribution that accounts for a substantial amount of counterion density.

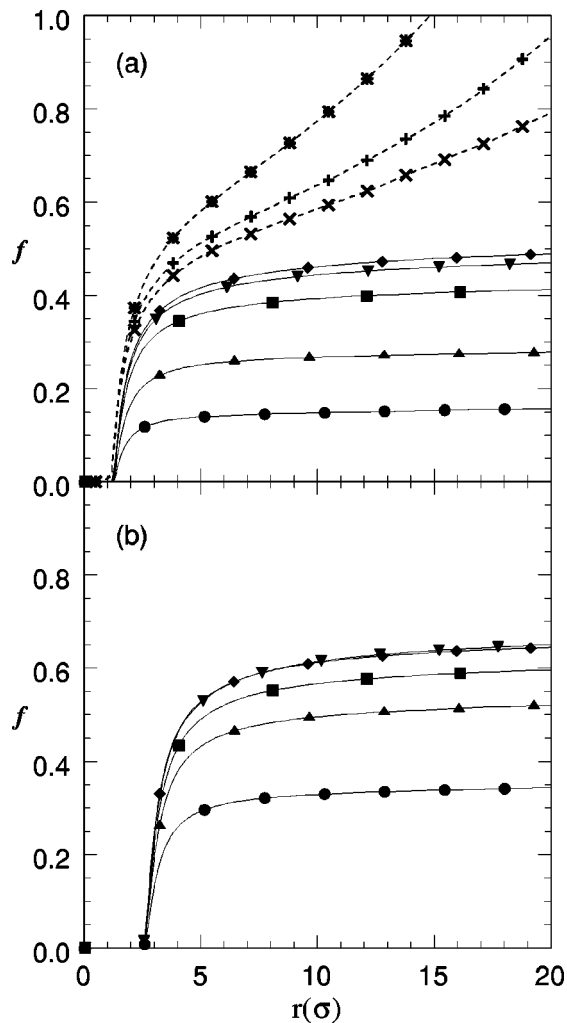


FIG. 4. The solid lines are the fraction of neutralizing condensed counterions, $f(r)$, within the shortest distance to the chain, r , for both ssDNA (a) and dsDNA (b). Symbols are as follows: $N=16$ (circles), $N=32$ (up triangles), $N=64$ (boxes), $N=128$ (down triangles), $N=256$ (diamonds). Dashed lines in Fig. 4(a) are for $N=20$ chains of ssDNA with salt [5 mM salt (x), 10 mM salt (+), and 20 mM salt (*)], where the fraction of neutralization can exceed unity due to the excess of counterions, and where coion counter-neutralization is not shown.

A more direct calculation of the fraction of condensed counterions is shown in Fig. 4. The distance r from a counterion to the chain is defined as the minimum of all distances from the counterion to any monomer of the chain. The time-averaged number of counterions within r is calculated and normalized by N to give $f(r)$, the fraction of counterions within a distance r . The number of condensed counterions is not a uniquely defined quantity.²³ The simple physical picture of condensed counterions has the electrostatic interactions trapping and holding these counterions within a short distance of the chain. The plots of $f(r)$ show that in salt-free solution a plateau is reached once $r \geq 3d$ and is maintained at least up to $r=20\sigma$. Looking at these plateau values in Fig. 4 we see that they increase with N . For dsDNA, the largest N are identical giving a large N limit for the plateau value to be $f=0.60$. For ssDNA, the saturation limit is apparently just above the range of the data at about $f=0.50$. For comparison, the Manning condensation value for an infinite chain is

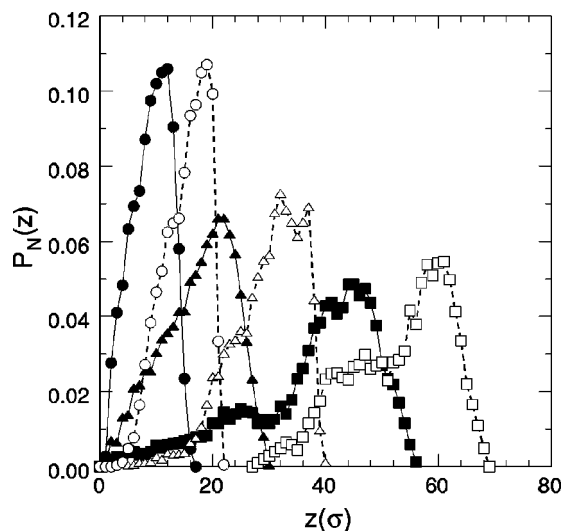


FIG. 5. The distribution of distances of the N th monomer from the grafting surface for ssDNA (solid lines) and dsDNA (dashed lines). The probabilities per unit length, P_N , that the end monomer will be found a given distance, z , from the surface are plotted for the $N=16$ (circles), $N=32$ (triangles), and $N=64$ (boxes) chains.

0.76 for dsDNA and 0.52 for ssDNA. The Manning calculation uses the Debye–Hückel equation, which breaks down for strong polyelectrolytes such as DNA and is for free, rather than grafted, polyelectrolytes. Nonetheless, it gives a good first approximation. The simulation data shows that there is a strong N dependence in the fraction of condensed counterions and that the infinite chain limit is reached for $N \approx 100$ for dsDNA and about twice as large for ssDNA.

The effect of added salt is included in Fig. 4(a). The chain and salt counterions are identical. In the Debye–Hückel theory, added salt is excluded from the condensation regime.²⁴ However, we find that adding salt increases the fraction of condensed counterions. In fact, for 20 mM salt, enough counterions for complete neutralization of the chain can be found within 15σ . This result is consistent with results of simulations of free chains in salt.²⁵ The system prefers to achieve a more uniform charge density, and in the presence of salt does so. This can be seen in Fig. 2(c), which shows that the net counterion distribution (with coions subtracted) is almost identical to the monomer distribution.

The orientation of the DNA chain can be examined through the position of the free end monomer. Figure 5 shows the distribution of the position of the N th monomer as a function of distance from the grafting surface, $P_N(z)$, for ssDNA and dsDNA for $N=16$, 32, and 64. In all cases, the dsDNA peak is at larger z than the peak in the ssDNA distribution, because dsDNA is stiffer. Although it is possible for the dsDNA chains to lay flat on the grafting surface, the simulation results indicate that this rarely occurs, and that for larger N becomes more rare if it happens at all. This is in part because conformations with the grafted chain perpendicular to the wall allow larger counterion entropy than for a chain laying flat on the grafting surface with only half of the volume around the chain accessible to the counterions.

IV. DISCUSSION

Csajka and Seidel (CS)¹⁴ have performed simulations of polyelectrolyte brush using almost the same model with different parameters. Their parametrization has $\sigma=9.8 \text{ \AA}$, which is about 3 times larger than for our ssDNA model. Their value of the Manning parameter ξ is 0.74, which is below the Manning condensation limit in contrast to either DNA system. This value of ξ is in the region where the Coulomb and thermal interactions are about equal, which puts the system intermediate between strong and weak polyelectrolytes.

We can compare our ssDNA results to the CS brush results, since both are flexible polyelectrolytes. Our system would correspond to the low grafting density limit. However, for $N=30$ as the grafting density decreases so does the brush height in the CS simulations. In fact, for the lowest density the average single chain structure in the brush is close to that of a neutral chain in solution, i.e., not extended like a highly charged polyelectrolyte. In contrast, we find the single, grafted ssDNA is highly extended. Since ξ is larger for ssDNA than for the CS chain, this would result in a more extended chain for ssDNA, but only by a small fraction. In solution, the polyelectrolyte chains with parameters very close to those of CS monotonically become more extended with decreasing density.⁷ Calculations by Csajka *et al.*¹⁵ predict a new brush phase, the collapsed brush, in the polyelectrolyte brush phase diagram. The lowest grafting density treated by CS is much larger than our equivalent density. As the grafting density is decreased from this lowest density to our dilute limit, our results indicate that the chains must at some point become more extended. This should be true for any strong polyelectrolyte since the single, grafted chain limit is not much different from a single chain in solution limit. The main difference between the brush state and the dilute state is that the counterion distribution in the brush is contained within the brush, whereas a significant portion lies beyond the chain length in the single chain limit. It will be interesting to determine the crossover point for the ssDNA brush where the counterions become contained within the brush and to determine where the collapsed brush state exists for the ssDNA parameters. If so, this would have consequences for DNA microarray and other technologies.

V. CONCLUSION

We have examined the structure of a single, grafted polyelectrolyte, specifically ssDNA and dsDNA, using coarse-grained MD simulations. A chain length dependence to the counterion condensation is found that is relevant to many applications since rather short DNA molecules are used. The counterion distribution extends beyond the chain volume in all cases. Even for the long chains where counterion condensation is maximal, there is a significant fraction of counterions beyond the corresponding brush height. In this dilute limit the chains are highly extended; in the case of dsDNA, this is true because the chain lengths studied are less than its persistence length. The ssDNA, which has a small intrinsic persistence length, is also highly extended in the

zero salt simulations. However, added salt does shrink the chain as salt ions do enter the volume near the chain.

ACKNOWLEDGMENTS

This work was supported by the DOE under Contract No. DE-AC04-94AL85000. Sandia is a multiprogram laboratory operated by Sandia Corp., a Lockheed Martin Company, for the DOE.

¹A. Steel, R. Levicky, T. Herne, and M. Tarlov, *Biophys. J.* **79**, 975 (2000).

²T. Herne and M. Tarlov, *J. Am. Chem. Soc.* **119**, 8916 (1997).

³D. Napper, *Polymeric Stabilization of Colloidal Dispersions* (Academic, London, 1983).

⁴A. Dunker, C. Brown, J. Lawson, L. Iakoucheva, and Z. Obradovic, *Biochemistry* **41**, 6573 (2002).

⁵S. Kumar, X. Yin, B. Trapp, J. Hoh, and M. Paulaitis, *Biophys. J.* **82**, 2360 (2002).

⁶J. Bright, M. Stevens, J. Hoh, and T. Woolf, *J. Chem. Phys.* **115**, 4909 (2001).

⁷M. Stevens and K. Kremer, *J. Chem. Phys.* **103**, 1669 (1995).

⁸M. Stevens, *Biophys. J.* **80**, 130 (2001).

⁹S. Miklavic and S. Marcelja, *J. Phys. Chem.* **92**, 6718 (1988).

¹⁰S. Misra, S. Varanasi, and P. Varanasi, *Macromolecules* **22**, 5173 (1989).

¹¹P. Pincus, *Macromolecules* **24**, 2912 (1991).

¹²O. Borisov, T. Birshtein, and E. Zhulina, *J. Phys. II* **1**, 521 (1991).

¹³R. Israels, F. Leermakers, G. Fleer, and E. Zhulina, *Macromolecules* **27**, 3249 (1994).

¹⁴F. Csajka and C. Seidel, *Macromolecules* **33**, 2728 (2000).

¹⁵F. Csajka, R. Netz, C. Seidel, and J.-F. Joanny, *Eur. Phys. J. E* **4**, 505 (2001).

¹⁶H. Chen, R. Zajac, and A. Chakrabarti, *J. Chem. Phys.* **104**, 1579 (1996).

¹⁷Y. Mir, P. Auroy, and L. Auvray, *Phys. Rev. Lett.* **75**, 2863 (1995).

¹⁸S. A. Sukhishvili and S. Granick, *Langmuir* **13**, 4935 (1997).

¹⁹Y. Tran and P. Auroy, *J. Am. Chem. Soc.* **123**, 3644 (2001).

²⁰E. L. Pollock and J. Glosli, *Comput. Phys. Commun.* **95**, 93 (1996).

²¹I. Yeh and M. Berkowitz, *J. Chem. Phys.* **111**, 3155 (1999).

²²P. Crozier, R. Rowley, and D. Henderson, *J. Chem. Phys.* **113**, 9202 (2000).

²³M. Deserno, C. Holm, and S. May, *Macromolecules* **33**, 199 (2000).

²⁴G. Manning, *Q. Rev. Biophys.* **11**, 179 (1978).

²⁵M. Stevens and S. Plimpton, *Eur. Phys. J. B* **2**, 341 (1998).